UAV quadrotor attitude control: An ADRC-EMC combined approach

UAV Quadrotor Attitude Control: an ADRC-EMC Combined Approach

Mauricio Alejandro Lotufo[2], Luigi Colangelo[1,*], Carlos Perez-Montenegro[1,*], Enrico Canuto[1,*], Carlo Novara[1,*]

Abstract

This study presents an original approach to the design of a complete digital attitude control unit for a UAV quadrotor. The approach is developed within the framework of Active Disturbance Rejection Control (ADRC) and Embedded Model Control (EMC), two well-established control design methodologies, both based on the estimation of the disturbances/uncertainties affecting the plant to control, and on their online cancellation. The attitude control design carried out in this paper demonstrates the possibility of adopting a simple input-output model to control the UAV attitude, while relying on the disturbance rejector to bridge the gap between model and plant reality. The designed attitude control unit encompasses an attitude state predictor, a control law, and a model-based reference generator. A multi-step test strategy is proposed to assess the performance of this disturbance-rejection-based attitude controller. Consequently, the presented experimental results are obtained both using a high-fidelity numerical simulator and in several experimental tests, carried out either on a laboratory single-axial test-bench or in-flight. Finally, the control unit performance is benchmarked, in simulation, against a state-of-the-art high-performance UAV attitude controller.

Keywords: UAV, Quadrotor, Attitude, Active Disturbance rejection, Embedded Model Control
2017 MSC: 00-01, 99-00

1. Introduction

The work presented in this paper is part of the Borea project (see [1]), whose main goal consists in developing a spacecraft emulator for testing guidance, navigation, and control strategies to be employed in space applications. The project is based on the cradle-to-grave design of a four-rotor vertical take-off

*Corresponding Author. Email: luigi.colangelo@polito.it
[1]Politecnico di Torino (Italy).
[2]Modelway s.r.l (Italy).

and landing (VTOL) aerial robot, namely a quadrotor aircraft; with no-tilting rotors.

Generally speaking, the attitude stabilization is a primary concern for the control designers addressing Unmanned Aerial Vehicles (UAVs), and particularly the quadrotors. Indeed, due to their under-actuated nature, quadrotors position control is performed by controlling the attitude angles.

In the literature, several approaches were studied in order to control the quadrotor attitude trajectories, during displacements or manoeuvres. For instance, Mahony et al. in [2] leveraged a set of sensors to provide an estimate of the absolute attitude of the vehicle, and the attitude controller is the intermediate loop of a hierarchical structure. In [3] an augmented PD attitude controller that guarantees exponential stability was developed. Also inner-outer control schemes were largely adopted, as in [4] and [5], while Bolandi et al. [6] addressed the attitude control problem via an optimized PID controller. Further, a high performance cascaded augmented PID controller is proposed by [7], based on Lie Group and Lie Algebra theory.

However, these state-of-the-art approaches may show limitations due to their difficulty in dealing with large disturbances, significant model uncertainties, or strong non-linearities (real quadrotors are typically affected by these kinds of issues). Indeed, in the presence of relevant disturbances, non-linearities, or uncertainties (that are not systematically accounted for by the "standard" methods), the control performance may deteriorate significantly, leading sometimes also to unstable behaviours.

In this paper, these problems are overcome by means of disturbance-rejection-based approaches. Generally speaking, disturbance rejection is a significant research area in control theory and practice. In this framework, several research contributions have been proposed, including Active Disturbance Rejection Control (ADRC) [8], disturbance observer-based control [9], also with a non-linear [10] or adaptive [11] formulations, or extended high-gain observer-based control [12], and Embedded Model Control (EMC) [13].

The main idea of ADRC [14] consists in reducing the plant, being either linear or non-linear, with state-feedback, to a cascade of integrators, allowing a standardized control design. In addition, a disturbance rejector, in parallel to the reduced plant, is aimed at nullifying the disturbance effects on the plant behaviour [15].

Also EMC [16] is based on the online estimation of the disturbances affecting the system to control, and the rejection of these disturbances. In particular, the EMC methodology envisages the design of a model-based digital control unit, based on an internal model of the plant to be controlled. One of the most interesting aspects of EMC consists in the capability of managing a large class of disturbance dynamics, low-frequency modelling errors, and unknown non-linearities, allowing their estimation and rejection by means of a relatively simple control law. Due to these features, the two approaches are strongly related.

In this paper, we develop an original ADRC-EMC algorithm for the design of a complete digital attitude control unit for a UAV quadrotor. As a

result, the complex UAV attitude control is recast into a simpler problem via a direct and active estimation and rejection of the generalized disturbance dynamics [17]. The designed control unit encompasses an attitude state predictor, which includes a disturbance estimator, a control law (with a disturbance rejection term), and a model-based reference generator. The algorithm is tested first using a high-fidelity numerical simulator, then in several experimental tests; some of them carried out on a laboratory single-axial test-bench, others carried out directly in-flight. The control unit performance is also benchmarked, in simulation, against a state-of-the-art high-performance UAV attitude controller. These tests show that the combined ADRC-EMC approach can be quite effective for a quadrotor attitude control, allowing a performance level (for instance, in terms of precise reference tracking under persisting external disturbances) that is hardly reached by the "standard" approaches.

The paper is organized as follows: after a general introduction, we lay the groundwork for the design methodology, in Sec. 2. The modelling of the quadrotor attitude, together with the complete design of the digital control unit, is addressed in Sec. 3. Then, in Sec. 4, the wide range of experimental tests of the developed attitude controller are reported and discussed. Finally, some conclusions are drawn in Sec. 5.

2. The Active Disturbance Rejection Control Philosophy

In this section, we introduce the most relevant aspects of the control design principles envisaged in this study. As mentioned above, the UAV quadrotor attitude control problem was approached from a disturbance rejection perspective. Such an approach is gaining more and more centrality in control engineering applications, due to its potential impact in addressing several practical control engineering problems. In this study, such a novel approach was creatively leveraged to achieve an end-to-end design of a UAV attitude controller, and somehow to bridge the theory-practice gap often affecting the automatic control field [8].

The disturbance rejection is accounted as the ultimate problem of the automatic controls, in the Active Disturbance Rejection Control (ADRC) [15]. ADRC relies on the idea that, for the purpose of controlling a linear or nonlinear physical process, striving to achieve a complete mathematical model is both impractical and unnecessary [15]. Conversely, the controller is designed against a controllable model, also called canonical model, and is fixed; whereas any difference between the plant and the canonical model is interpreted as disturbance, to be real-time estimated and rejected. These active disturbance estimation and cancellation allow the ADRC design methodologies not to require a great knowledge of the plant dynamics, thus notably increasing the practical applicability of the devised design solution. Indeed, due to the action of the rejector module, the plant physics is forced to behave like the canonical model, which becomes the basis for the control law straightforward design.

To this aim, ADRC adopts the notion of generalized disturbance f to describe all the plant uncertainties, thus both the internal dynamics and the external disturbances. However, no explicit analytical expression for f is required,

as long as we have a reliable estimate to perform an active cancellation of such a term. As a result, the ADRC approach introduces a substantial reduction in the complexity of the problem, since the order of the system and an approximate value of the command gain are the only factors to be known.

In this context, the ADRC leverages an extended-state observer. The typical ADRC observer is characterized by an augmented state model, where an extra state variable is introduced to track the generalized disturbance behaviour and to provide a reliable estimate $\hat{f}$ to the rejector. In turn, this implies a two degrees of freedom control structure [13]: one for the uncertainty compensation, while the other regulates the closed-loop performance.

2.1. New Perspectives for ADRC: the Embedded Model Control Framework and the Combined Approach

Within the overall framework of the ADRC techniques, in this study the attitude control problem is tackled through the Embedded Model Control (EMC) perspective [18].

An EMC digital control unit consists in three main elements (see Fig. 1): (i) the state predictor, based on an internal (or embedded) model of the plant to be controlled, plus the noise estimator (output-to-state feedback, in Fig. 1), (ii) a reference generator (or guidance), which provides the reference command and the reference controllable states, and (iii) the control law.

In turn, the internal model of the plant is made up by two parts (see Fig. 1): the controllable canonical model, namely the simplified input-output model of the plant dynamics, and a disturbance dynamics. This disturbance dynamics, playing the role of the above-mentioned rejector, is a dynamic model of the unknown disturbances and parameter uncertainties, potentially affecting the plant, not included into the controllable input-output model.

Interestingly, this EMC peculiar perspective on the ADRC approach let us introduce three notable distinctive traits into the typical ADRC-based control unit design.

First of all, according to [13], the control unit was tailored to the UAV specific application, by introducing a rejector structure fitting the class of control problems to be addressed. Indeed, differently from the standard ADRC solution, we built a second-order dynamic rejector (cf. disturbance dynamics in Fig. 1). Such a design choice allowed a greater disturbance rejection capability, in the low frequency band of interest.

Secondly, although the ADRC considers all the plant disturbances as lumped into the same input channel (uncertainty feedback scheme [13]), in this study we also accounted for a command-dependant fractional error dynamics, due to the neglected dynamics, directly acting on the plant output [13, 18]. This choice allowed our design model to match closely the physics of the plant to be controlled. Also, it brought to a finer frequency design and tuning of the state predictor, substantially enhancing the closed-loop stability of the control unit by dismissing the command-dependent effects from the rejector.

Thirdly, concerning the disturbance rejection, the EMC architecture allowed us to deal also with input disturbances channels not necessarily acting at the

command level (non-collocated), by adopting a peculiar definition of the tracking error, as per (15).

As a result, the EMC more comprehensive disturbance dynamics as well as its disturbance rejection control law were leveraged to build a combined ADRC-EMC architecture, with the purpose to extend the capabilities and performance of the ADRC basic structure. To this aim, starting from their multiple linking points, ADRC and EMC were combined by properly re-framing the EMC design structure and tools in the ADRC scenario. Consequently, henceforth we will refer to the combined ADRC-EMC control design.

3. UAV Quadrotor Attitude Control via ADRC-EMC

In this section the quadrotor attitude modelling, leading to the digital control unit design, and the control unit design itself are presented, within the combined ADRC-EMC framework.

3.1. Quadrotor Attitude Modelling

The model of the quadrotor attitude kinematics was addressed through the Euler angles representation, collected in $\boldsymbol{\chi} = \{\phi,\ \theta,\ \psi\}$, and describing respectively the UAV roll, pitch, and yaw motions. Specifically, by selecting the Euler angles sequence $3-2-1$, the body-to-inertial attitude matrix $R_b^i(\boldsymbol{\chi})$ holds:

$$R_b^i(\boldsymbol{\chi}) = Z(\psi)Y(\theta)X(\phi) = \begin{bmatrix} c_\psi c_\theta & -s_\psi & c_\psi s_\theta \\ s_\psi c_\theta & c_\psi & s_\psi s_\theta \\ -s_\theta & 0 & c_\theta \end{bmatrix} X(\phi), \tag{1}$$

where, as henceforth in this paper, given a generic angle α, c_α, s_α, and t_α, stand respectively for the $\cos\alpha$, $\sin\alpha$, and $\tan\alpha$, functions. Based on the rotation matrix in (1), the well-known rigid-body attitude kinematics was defined as follows [19]:

$$\begin{aligned} \dot{\boldsymbol{\chi}}(t) &= A(\boldsymbol{\chi}(t))\boldsymbol{\omega}_b(t), \\ A(\boldsymbol{\chi}) &= \begin{bmatrix} 1 & s_\phi t_\theta & c_\phi t_\theta \\ 0 & c_\phi & -s_\phi \\ 0 & s_\phi/c_\theta & c_\phi/c_\theta \end{bmatrix} = \begin{bmatrix} 1 & 0 & t_\theta \\ 0 & 1 & 0 \\ 0 & 0 & 1/c_\theta \end{bmatrix} X(\phi), \end{aligned} \tag{2}$$

where $\boldsymbol{\omega}_b$ is the quadrotor body angular rate vector and $A(\boldsymbol{\chi})$ is the kinematic matrix.

Consequently, the input-output model of the quadrotor attitude was obtained by computing the time derivative of the Euler kinematics (2), namely:

$$\ddot{\boldsymbol{\chi}}(t) = \dot{A}(\boldsymbol{\chi}(t))\boldsymbol{\omega}_b(t) + A(\boldsymbol{\chi}(t))\dot{\boldsymbol{\omega}}_b(t), \tag{3}$$

where:

$$\dot{A}(\boldsymbol{\chi}(t)) = \dot{\theta} \begin{bmatrix} 0 & 0 & 1/c_\theta^2 \\ 0 & 0 & 0 \\ 0 & 0 & s_\theta/c_\theta^2 \end{bmatrix} X(\phi) + \\ + \dot{\phi} \begin{bmatrix} 1 & 0 & t_\theta \\ 0 & 1 & 0 \\ 0 & 0 & 1/c_\theta \end{bmatrix} X(\phi). \tag{4}$$

To complete (3), let us now consider the quadrotor attitude dynamics, including the gyroscopic effects, viz.:

$$\dot{\boldsymbol{\omega}}_b(t) = J^{-1}(\mathbf{u}_m(t) - \boldsymbol{\omega}_b(t) \times J\boldsymbol{\omega}_b(t) + \mathbf{d}(t)), \tag{5}$$

where $\mathbf{u}_m$ is the command torque along the three body axes, $\mathbf{d}$ represents all the external disturbances, while J is the quadrotor inertia matrix. Finally, the model fidelity was strengthened by considering also the actuator dynamics. Specifically, the actuator dynamics was proven to be reliably described as [20]:

$$\dot{\mathbf{u}}_m(t) = -p\mathbf{u}_m(t) + p\mathbf{u}(t), \tag{6}$$

where $\mathbf{u}$ is the command input to the plant, while p is the actuator pole. As a result, by combining (6) and (5) with (3), the continuous-time quadrotor attitude model holds:

$$\begin{aligned} \dot{\mathbf{x}}_1(t) &= \mathbf{x}_2(t), \quad \mathbf{x}_1(0) = \mathbf{x}_{10}, \\ \dot{\mathbf{x}}_2(t) &= A(\mathbf{x}_1(t))J^{-1}(\mathbf{x}_3(t) + \mathbf{h}(\mathbf{x}(t)) + \mathbf{d}(t)), \quad \mathbf{x}_2(0) = \mathbf{x}_{20}, \\ \dot{\mathbf{x}}_3(t) &= -p\mathbf{x}_3(t) + p\mathbf{u}(t), \quad \mathbf{x}_3(0) = \mathbf{x}_{30}, \\ \mathbf{y}(t) &= A(\mathbf{x}_1(t))^{-1}\mathbf{x}_2(t), \quad \mathbf{z}(t) = \mathbf{x}_1(t). \end{aligned} \tag{7}$$

In (7), $\mathbf{y}$ and $\mathbf{z}$ are the measure and the performance variables, respectively, and:

$$\begin{aligned} \mathbf{x}(t) &= \begin{bmatrix} \mathbf{x}_1 \\ \mathbf{x}_2 \\ \mathbf{x}_3 \end{bmatrix}(t) = \begin{bmatrix} \boldsymbol{\chi} \\ \dot{\boldsymbol{\chi}} \\ \mathbf{u}_m \end{bmatrix}(t), \\ \mathbf{h}(\mathbf{x}(t)) &= JA(\mathbf{x}_1(t))^{-1}\dot{A}(\mathbf{x}_1(t))\boldsymbol{\omega}_b(t) - \boldsymbol{\omega}_b(t) \times J\boldsymbol{\omega}_b(t), \\ \boldsymbol{\omega}_b(t) &= A(\mathbf{x}_1(t))^{-1}\mathbf{x}_2(t). \end{aligned} \tag{8}$$

In (8), the non-linear term $\mathbf{h}(\mathbf{x})$ collects the quadrotor dynamics effects linked to the Euler matrix derivative as well as the gyroscopic effects.

Finally, concerning the model validity, $A(\mathbf{x}_1)$ was considered to be always invertible; for the purpose of this study. Indeed, the admissible manoeuvres, driving the attitude control performance, will require values of the tilt angles much smaller than the singularity condition eventually causing gimbal lock situations (i.e. 45° is considered a large angle, for the purpose of this study).

3.2. The ADRC-EMC Digital Control Unit

For the purpose of the digital control unit design, the decoupled model in (7) was considered, while the effects of the attitude coupling, whereas not included in $\mathbf{h}(\mathbf{x})$, were estimated as unknown disturbances ($\overline{\mathbf{d}}$, in Fig. 1) to be ultimately rejected. As a result the effectiveness of an independent single-axis attitude control design is enhanced. However, although the three single-axis independent controllers will have the same architecture, the gains tuning and the controller bandwidths will unveil the differences among them; due to the axial-specific properties like inertia and couplings factors (cf. Table 1).

3.2.1. The Internal Model

The first step to derive the ADRC-EMC digital control unit consists in building its core part: the discrete-time (DT) internal model. Originating from the EMC design, the internal model of the UAV quadrotor is intended to be directly implemented on the Borea UAV, and is based on the continuous-time design model detailed in (7). To this aim, (7) was converted in discrete-time, by means of an Euler-forward discretisation, viz.:

$$\begin{aligned}
\mathbf{x}_1(i+1) &= \mathbf{x}_1(i) + \mathbf{x}_2(i), \quad \mathbf{x}_1(0) = \mathbf{x}_{10}, \\
\mathbf{x}_2(i+1) &= \mathbf{x}_2(i) + \mathbf{x}_3(i) + A(\mathbf{x}_1(i))J^{-1}(\mathbf{h}(\mathbf{x}(i)) + T^2\mathbf{d}(i)), \ \mathbf{x}_2(0) = \mathbf{x}_{20}, \\
\mathbf{x}_3(i+1) &= (1-\beta)\mathbf{x}_3(i) + \beta T^2 A(\mathbf{x}_1(i))J^{-1}\mathbf{u}(i), \quad \mathbf{x}_3(0) = \mathbf{x}_{30}, \\
\mathbf{y}(i) &= T^{-1}A(\mathbf{x}_1(i))^{-1}\mathbf{x}_2(i), \quad \mathbf{z}(i) = \mathbf{x}_1(i).
\end{aligned} \tag{9}$$

In (9), T is the DT control step, in seconds, and $\beta = pT$ is the actuator dynamics eigenvalue. To streamline the further design steps, let us simplify (9) by defining the following transformations:

$$\begin{aligned}
\overline{\mathbf{h}}(\mathbf{x}(i)) &= A(\mathbf{x_1}(i))J^{-1}\mathbf{h}(\mathbf{x}(i)), \quad \overline{\mathbf{d}}(\mathbf{x_1}(i), i) = T^2 A(\mathbf{x_1}(i))J^{-1}\mathbf{d}(i), \\
\overline{\mathbf{u}}(i) &= T^2 A(\mathbf{x_1}(i))J^{-1}\mathbf{u}(i), \quad \overline{\mathbf{y}}(i) = TA(\mathbf{x_1}(i))\mathbf{y}(i).
\end{aligned} \tag{10}$$

Hence, the DT quadrotor attitude model (9) shrinks to:

$$\begin{aligned}
\mathbf{x}_1(i+1) &= \mathbf{x}_1(i) + \mathbf{x}_2(i), \quad \mathbf{x}_1(0) = \mathbf{x}_{10}, \\
\mathbf{x}_2(i+1) &= \mathbf{x}_2(i) + \mathbf{x}_3(i) + \overline{\mathbf{h}}(\mathbf{x}(i)) + \overline{\mathbf{d}}(\mathbf{x_1}(i), i), \quad \mathbf{x}_2(0) = \mathbf{x}_{20}, \\
\mathbf{x}_3(i+1) &= (1-\beta)\mathbf{x}_3(i) + \beta\overline{\mathbf{u}}(i), \quad \mathbf{x}_3(0) = \mathbf{x}_{30}, \\
\overline{\mathbf{y}}(i) &= \mathbf{x}_2(i), \quad \mathbf{z}(i) = \mathbf{x}_1(i),
\end{aligned} \tag{11}$$

being $\overline{\mathbf{h}}(\mathbf{x}(i))$ and $\overline{\mathbf{d}}(\mathbf{x_1}(i), i)$ the known (deterministic) and the unknown disturbance terms, respectively. As a result, the equations (11) provide the final DT input-output controllable model (canonical model, in Fig. 1), on which the digital controller design was based. The state variables are: the attitude angles $\mathbf{x}_1$, the angular rate $\mathbf{x}_2$, and the identified equivalent actuator dynamics $\mathbf{x}_3$; coherently with $\mathbf{x}$ in (8).

Finally, to complete the internal model, the plant input-output description in (11) must be paired with the generic disturbance estimation dynamics, namely the ADRC-EMC rejector (cf. Fig. 1).

3.2.2. From the ADRC-EMC Rejector Disturbance Dynamics to the Attitude Predictor

To build the ADRC-EMC rejector, augmenting the DT input-output model (11), a second-order stochastic disturbance dynamics (Fig. 1) was devised, i.e.:

$$\begin{aligned} \mathbf{x}_{d1}(i+1) &= \mathbf{x}_{d1}(i) + \mathbf{x}_{d2}(i) + \overline{\mathbf{w}}_2(i), \quad \mathbf{x}_{d1}(0) = \mathbf{x}_{d10}, \\ \mathbf{x}_{d2}(i+1) &= \mathbf{x}_{d2}(i) + \overline{\mathbf{w}}_3(i), \quad \mathbf{x}_{d2}(0) = \mathbf{x}_{d20}, \\ \overline{\mathbf{d}}(i) &= \mathbf{x}_{d1}(i) + \overline{\mathbf{w}}_1(i). \end{aligned} \tag{12}$$

It is worthwhile to notice how, according to the EMC typical architecture, the disturbance dynamics (12) is driven by a noise vector $\overline{\mathbf{w}} = \{\overline{\mathbf{w}}_0, \overline{\mathbf{w}}_1, \overline{\mathbf{w}}_2, \overline{\mathbf{w}}_3\}$, whose components $\overline{\mathbf{w}}_k$ are functions of the model error $\overline{\mathbf{e}}_m = \overline{\mathbf{y}} - \mathbf{x}_2$ (measurement minus estimate). As a matter of fact, $\overline{\mathbf{w}}$ lets us close the loop via an output-to-state feedback, in order to build the final state predictor to be directly coded into the UAV control unit; as depicted in Fig. 1.

In this case, to achieve the closed-loop stabilization of the model, $\overline{\mathbf{w}}$ was designed as a static feedback, with a suitable dimension, i.e.:

$$\overline{\mathbf{w}}(i) = \begin{bmatrix} \overline{\mathbf{w}}_0 \\ \overline{\mathbf{w}}_1 \\ \overline{\mathbf{w}}_2 \\ \overline{\mathbf{w}}_3 \end{bmatrix}(i) = \begin{bmatrix} L_0 & 0 & 0 & 0 \\ 0 & L_1 & 0 & 0 \\ 0 & 0 & L_2 & 0 \\ 0 & 0 & 0 & L_3 \end{bmatrix} \overline{\mathbf{e}}_m(i), \tag{13}$$

where $L_k = \{\dots, l_{kj}, \dots\}$, $k = 0, \dots, 3$, $j = x, y, z$, are the closed-loop predictor gain vectors to be designed and tuned, as per below.

As a result, by gathering (11), (12), and (13), we obtain the generic 3D DT state predictor sketched in Fig. 1 which, restricted to the single-axis case (dropping the j-th axis subscript), reads:

$$\begin{aligned} &\begin{bmatrix} x_1 \\ x_2 \\ x_3 \\ x_{d1} \\ x_{d2} \end{bmatrix}(i+1) = \begin{bmatrix} 1 & 1 & 0 & 0 & 0 \\ 0 & 1-l_1 & 1 & 1 & 0 \\ 0 & -\beta l_0 & 1-\beta & 0 & 0 \\ 0 & -l_2 & 0 & 1 & 1 \\ 0 & -l_3 & 0 & 0 & 1 \end{bmatrix} \begin{bmatrix} x_1 \\ x_2 \\ x_3 \\ x_{d1} \\ x_{d2} \end{bmatrix}(i) + \\ &+ \begin{bmatrix} 0 & 0 \\ 0 & l_1 \\ \beta & \beta l_0 \\ 0 & l_2 \\ 0 & l_3 \end{bmatrix} \begin{bmatrix} \overline{u} \\ \overline{y} \end{bmatrix}(i) + \begin{bmatrix} 0 \\ \overline{h}(\mathbf{x}(i)) \\ 0 \\ 0 \\ 0 \end{bmatrix}, \quad \begin{bmatrix} x_1 \\ x_2 \\ x_3 \\ x_{d1} \\ x_{d2} \end{bmatrix}(0) = \begin{bmatrix} x_{10} \\ x_{20} \\ x_{30} \\ x_{d10} \\ x_{d20} \end{bmatrix}. \end{aligned} \tag{14}$$

The actuator dynamics block describes the identified first-order actuator dynamics, characterized by a complementary eigenvalue $\beta = 0.276$; coherently with the results obtained in [20]. Then, it is clear how the states x_{d1} and x_{d2} constitute the disturbance estimation dynamics of the ADRC-EMC rejector augmenting the canonical model.

As a result, the closed-loop model in (14) can be determined by four gains (l_0, l_1, l_2, l_3) to be tuned trading-off between the closed-loop stability and the

reference attitude tracking performance. In this study, the gains were preliminary tuned by fixing the closed-loop complementary eigenvalues γ_k, $k = 1, 2, 3, 4$, of the predictor state matrix coherently with the guidelines in [13], via a pole placement, and then refined in-flight.

To this aim, two main relevant factors for the eigenvalues tuning are the actuator dynamics, and the quadrotor physical properties. Hence, on one side, at least one of the complementary eigenvalues γ_k was placed at the same frequency of the actuator, in order not to modify the actuator dynamics, so to avoid command saturations. On the other side, a proper and specific tuning of each single-axis controller was crucial to account for the axis-wise differences; such as the quadrotor inertia or the attainable command authority. For the sake of completeness, the final state predictor closed-loop eigenvalues are listed in Table 1.

To conclude, concerning the model validity, let us notice that the angular position state variable, x_1, was placed out of the loop in (14). Indeed, differently from solutions combining the quadrotor body angular rate and acceleration [21], in this study only the angular rate measurement from the gyroscope was supposed available. As a matter of fact, this implies that the UAV attitude may drift, thus undermining the angular tracking performance of the ADRC-EMC control law. Therefore, the control unit was endowed with a COTS gyroscope with a sufficiently high bias stability, with respect to the specified mission scenarios (e.g. mission flight-time and manoeuvres' envelope). Such a design choice ensured a practically negligible attitude drift, as verified both in simulation and flight. Furthermore, the control algorithms include an automatic calibration procedure to estimate the gyroscope bias, before every take-off, and perform its compensation during the flight.

3.2.3. The ADRC-EMC Control Law

The ADRC-EMC control law is made up by four terms: (i) the feed-forward component $\underline{\mathbf{u}}$, called nominal command, (ii) the state feedback $K\mathbf{e}$, (iii) the disturbance rejection term $M\mathbf{x}_d$, and (iv) the deterministic disturbance $\overline{\mathbf{h}}(\mathbf{x})$. Ergo, the full command expression holds:

$$\begin{aligned} \mathbf{u}(i) &= \underline{\mathbf{u}}(i) + K\mathbf{e}(i) - M\mathbf{x}_d(i) - \overline{\mathbf{h}}(\mathbf{x}(i)), \\ \mathbf{e}(i) &= (\underline{\mathbf{x}}(i) - Q\mathbf{x}_d(i)) - \mathbf{x}(i), \quad \text{where} \\ Q &= \begin{bmatrix} 0 & 0 \\ 0 & 0 \\ 1 & 0 \end{bmatrix}, \quad M = \begin{bmatrix} 1 & 1/\beta \end{bmatrix}. \end{aligned} \tag{15}$$

In (15), $\underline{\mathbf{u}}$ is calculated by the reference generator algorithm, based on the current states and the operator's request, in order to minimize the feedback effort (see Fig. 1 and 3.2.4). On the other side, K is the feedback gains matrix, which was designed, by means of pole placement, in order to have asymptotically stable closed-loop eigenvalues (see Table 1 for the final values). Finally, $\mathbf{e}$ is the tracking error. According to the peculiar definition proposed in (15), the ADRC-

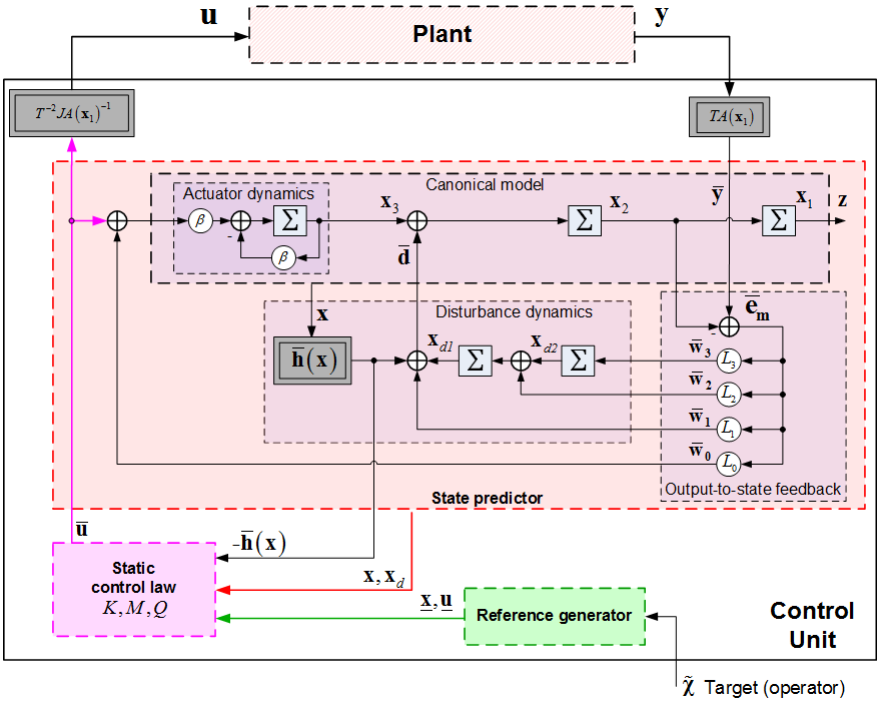

Figure 1: UAV quadrotor attitude digital control unit.

EMC tracking error is defined via the reference state vector $\underline{\mathbf{x}}$, and the canonical and the rejector states; $\mathbf{x}$ and $\mathbf{x}_d$, respectively.

The matrices Q and M are the result of the Sylvester-Francis equation, as outlined in [13], and allow the ADRC-EMC solution to extend the results of the standard ADRC design. Specifically, M allows to consider a disturbance dynamics of any order (second, in this case). On the other hand, Q let the disturbance $\mathbf{x}_d$ enter as a reference shifting, allowing to suitably discharge the feedback when non-collocated input disturbances apply. As a result, the ADRC-EMC architecture is able to correctly estimate, and reject, also input disturbances possibly not acting at the command level [16] (e.g. $\mathbf{x}_{d1}$ in Fig. 1).

Finally, it is worth to notice the design choice of including explicitly in the control law (15) the deterministic disturbance term $\overline{\mathbf{h}}(\mathbf{x})$, separately from the estimated disturbance $\mathbf{x}_d$; coherently with the model in (11). This implies the possibility to have a direct compensation of the deterministic non-linearities included in $\overline{\mathbf{h}}(\mathbf{x})$ (e.g. the gyroscopic effect), up to a large bandwidth. However, although relying on its mathematical formulation, the direct compensation of $\overline{\mathbf{h}}(\mathbf{x})$ is somewhat uncertain, due to: possible errors and noises, and the limited bandwidth of the command due to the actuator dynamics. Therefore, according to the ADRC-EMC design, a fraction of its effect will be anyway compensated by the estimated disturbance term $\mathbf{x}_d$ (cf. Fig. 6 and its description).

3.2.4. The Attitude Reference Generator

The aim of the attitude reference generator, or attitude guidance, consists in enabling a full, in-flight, three-axial, attitude control test capability. Indeed, as depicted in Fig. 1, the reference generator provides the control law (15) with: (i) the nominal command $\underline{\mathbf{u}}$, and (ii) the reference canonical states $\underline{\mathbf{x}} = [\underline{x}_1 \ \underline{x}_2 \ \underline{x}_3]^T$ to compute the tracking error $\mathbf{e}$.

Generally speaking, the guidance input is represented by the operator's request (here also called target). Specifically, in this study, the attitude reference generator was driven by the reference attitude $\tilde{\boldsymbol{\chi}} = \{\tilde{\phi}, \tilde{\theta}, \tilde{\psi}\}$; requested by the UAV operator and communicated to the on-board digital control unit via a radio control. As a matter of fact, the target angles in $\tilde{\boldsymbol{\chi}}$ set the UAV desired reference attitude, to be eventually tracked by means of the attitude controller.

From the design perspective, in line with our ADRC-EMC framework, we implemented a model-based design based on the same input-output controllable dynamics (11) of the state predictor, as sketched in Fig. 2. In short, this design model choice aimed at reducing significantly the feedback effort, since the reference state trajectories will be naturally compliant with the plant dynamics.

Consequently, recollecting the UAV input-output canonical model (11), the DT closed-loop state equations of the single-axis attitude guidance model read:

$$\begin{bmatrix} \underline{x}_1 \\ \underline{x}_2 \\ \underline{x}_3 \end{bmatrix}(i+1) = \begin{bmatrix} 1 & 1 & 0 \\ 0 & 1 & 1 \\ -\beta\underline{k}_1 & -\beta\underline{k}_2 & 1-\beta(1+\underline{k}_3) \end{bmatrix} \begin{bmatrix} \underline{x}_1 \\ \underline{x}_2 \\ \underline{x}_3 \end{bmatrix}(i) + \\ + \begin{bmatrix} 0 \\ 0 \\ \beta\underline{k}_1 \end{bmatrix} \tilde{\theta}(i), \quad \begin{bmatrix} \underline{x}_1 \\ \underline{x}_2 \\ \underline{x}_3 \end{bmatrix}(0) = \begin{bmatrix} \underline{x}_{10} \\ \underline{x}_{20} \\ \underline{x}_{30} \end{bmatrix}, \tag{16}$$
$$\underline{u}(i) = \begin{bmatrix} -\underline{k}_1 & -\underline{k}_2 & -\underline{k}_3 \end{bmatrix} \begin{bmatrix} \underline{x}_1 \\ \underline{x}_2 \\ \underline{x}_3 \end{bmatrix}(i) + \underline{k}_1\tilde{\theta}(i),$$

where $\tilde{\theta}$ stands for any generic attitude angle of $\tilde{\boldsymbol{\chi}}$ to be moved, the pitch in this case, and $\underline{u}$ is the reference command. As showed in Fig. 2, the guidance model (16) was made closed-loop and convergent through the gains $\underline{K} = \{\underline{k}_1, \underline{k}_2, \underline{k}_3\}$. The three closed-loop gains in $\underline{K}$ were computed by means of a pole placement procedure, by assuming the three closed-loop complementary eigenvalues $\underline{\gamma}_k$, $k = 1, 2, 3$, as coincident and placed at the same frequency of the identified actuator dynamics β. Such a design choice aimed to avoid command saturations due to the actuator dynamics. From this perspective, let us notice that the attitude guidance in (16) does not include any explicit constraint on $\underline{u}$, which is naturally bounded via a proper tuning of the closed loop eigenvalues. For the sake of completeness, the guidance closed-loop eigenvalues are listed in Table 1.

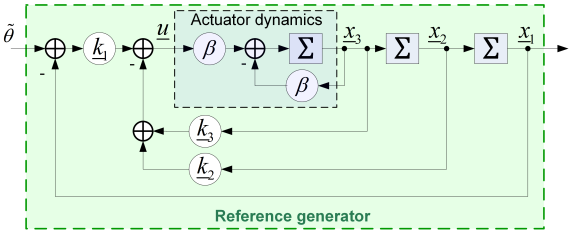

Figure 2: Quadrotor attitude reference generator.

4. Experimental Results

In this section the experimental tests of the quadrotor attitude control are presented. The attitude control test campaign consisted in several steps. Specifically, we performed: (i) high-fidelity simulations, and (ii) real UAV trials, either on a test-bench or in outdoor flight, encompassing different attitude manoeuvres and configurations.

In Table 1 the final controller parameters, fine-tuned via the simulation campaign and employed for the several experimental tests, are listed. The other relevant test parameters were either directly measured in-field or suitably indentified by the authors [20].

Table 1: Quadrotor ADRC-EMC attitude control: experimental tests parameters.

Parameter	Value
Control step [s]	0.020
Simulation step [s]	0.0005
Nominal inertia [kgm^2]	$\texttt{diag}\{0.04, 0.04, 0.06\}$
Nominal weight [kg]	2.5
UAV inter-axis [m]	0.5
Complementary Eigenvalues	
Actuator dynamics	0.276
Guidance (X-Y-Z axes)	0.276 0.276 0.276
Feedback (X-Y axes)	0.276 0.276 0.276
Feedback (Z axis)	0.027 0.069 0.0173
Predictor (X-Y axes)	0.276 0.300 0.400 0.500
Predictor (Z axis)	0.276 0.276 0.276 0.276

4.1. Test-bench Tests

The single-axis tilt attitude controllers were tested on a mono-axial experimental test-bench; designed on purpose (see Figure 3). The main objective of these test-bench experiments was the testing and tuning, in safety conditions, of the attitude tilt controllers, with respect to the reference tracking and the disturbance rejection purposes. From the measurement perspective, the quadrotor was endowed with a gyroscope, providing the angular rate measure, and an accelerometer, to measure the quadrotor rotational angle.

In the following, some results from the test-bench experiments considering a typical attitude pitch manoeuvre are provided. In Fig. 4 (top) the attitude angle trajectory tracking is shown. The attitude guidance (thin line) represents the reference angle $\underline{x}_1$ provided by the reference generator (16), to be tracked by the controller. As a result, the attitude angle estimated by the state predictor x_1 (dashed-thick line) is shown to follow the reference trajectory under the effect of the command action.

For completeness, Fig. 4 (bottom) also depicts the estimated tracking error $e = \underline{x}_1 - x_1$ (thick line), relatively to the trajectory showed in Fig. 4 (top). The maximum error magnitude is 0.022 rad, for a range of variations of the tilt angles close to 0.2 rad, as per Fig. 4 (top), that it was deemed coherent with the quadrotor displacement objectives. Further, from the attitude angle measurement $\tilde{x}_1$, via the accelerometer, it was computed the measured tracking error $\tilde{e} = \underline{x}_1 - \tilde{x}_1$, also depicted in Figure 4 (bottom, thin line). The measured tracking error $\tilde{e}$ is larger than the estimated one e, as expected, yet bounded and matching its low-frequency trend. Indeed, the estimated error, depending on the attitude estimate x_1, has a limited bandwidth with respect to the measurement $\tilde{x}_1$. In turn, the measured tracking error is obviously affected by high-frequency measurement errors.

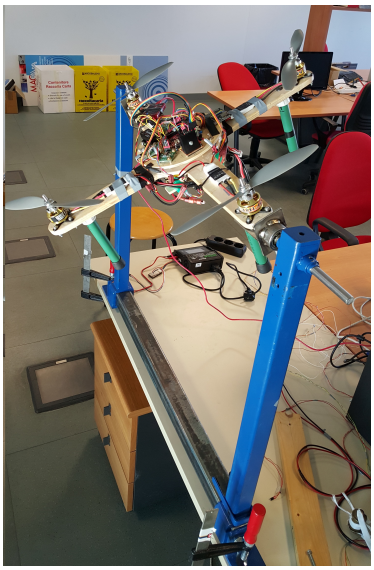

Figure 3: Experimental mono-axial test-bench for multirotor UAVs.

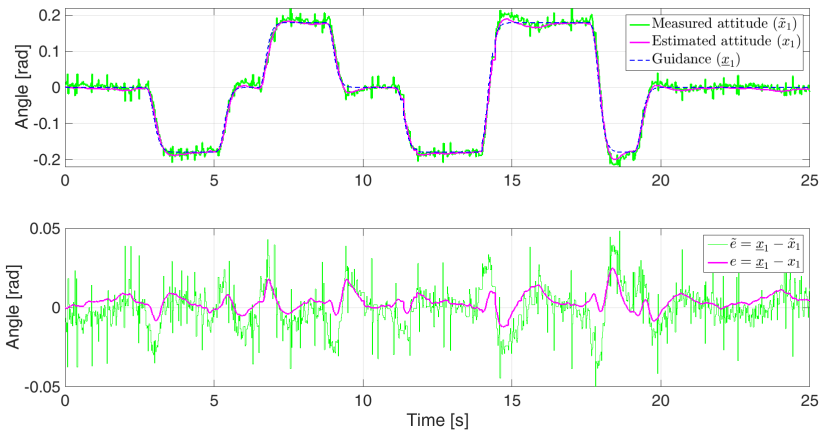

Figure 4: Single-axis attitude test-bench experiment: angle tracking (top), tracking errors (bottom).

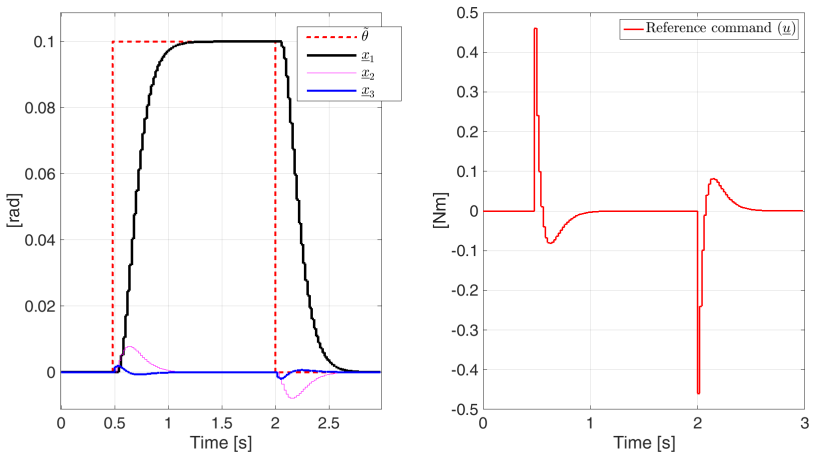

Figure 5: Attitude guidance simulation.

4.2. Simulation Tests

In parallel with the UAV trials, an extensive and multi-purpose simulation campaign was carried out. To this aim a high-fidelity Matlab/Simulink simulator was developed and validated by the authors, in the last few years (e.g. [1], [20]). Specifically, the Borea UAV simulator includes the quadrotor dynamics as well as the models of all the sensors available on-board (accelerometers, gyroscopes, magnetometer, and a differential GPS receiver). Also their errors (e.g. bias, drift) and noise are accounted for. All the sensor models were validated against their performance specifications, during on-purpose quadrotor flight tests (e.g. in [20]). Finally, the command quantization (12 bits) was also considered in the simulations presented below.

In the following, we report some of the most relevant results of the simulation tests about our disturbance-rejection-based attitude controller.

Preliminary, we focused on the guidance algorithm. In Fig. 5 (left) are reported the simulated guidance states, from (16), assuming the parameter values in Table 1, in case of a square wave target pitch angle $\tilde{\theta} = 0.1\,\text{rad}$, requested by the operator. On the other side, in Figure 5 (right) the calculated reference command $\underline{u}$ is shown to be far from saturation ($\underline{u}_{\max} \approx 1.5\,\text{N m}$). These results highlight the guidance block capability to drive the quadrotor attitude with a low feedback effort, while ensuring a suitable performance.

Following, a second simulation result concerns the disturbance estimation capabilities of the ADRC-EMC state predictor. As mentioned in 3.2.3, $\overline{\mathbf{h}}(\mathbf{x})$ was explicitly included both in the predictor (14) and in the control law (15). Such a design choice aimed to distinguish the deterministic effects in $\overline{\mathbf{h}}(\mathbf{x})$ from the (unknown) disturbances, estimated by the rejector ($\overline{\mathbf{d}}(\mathbf{x}_1)$, in (11)), in order for having a direct compensation of $\overline{\mathbf{h}}(\mathbf{x})$, up to a large bandwidth. However, being $\overline{\mathbf{h}}(\mathbf{x})$ uncertain at some extent, a fraction of its effect will be included

anyway by the unknown disturbance. To clarify such a concept, in Fig. 6, given the simulated $\overline{\mathbf{h}}(\mathbf{x})$ (thin line), it is shown how the estimated disturbance signal $\mathbf{x}_{d1}$, provided by the rejector, may have two different trends. As a matter of fact, it will include the effects of $\overline{\mathbf{h}}(\mathbf{x})$, in case such non-linear term is not explicitly defined in the model (thick line). Otherwise, if $\overline{\mathbf{h}}(\mathbf{x})$ is explicitly modelled (as chosen in this study), the rejector disturbance signal results to be discharged by the $\overline{\mathbf{h}}(\mathbf{x})$ value (dashed line). In this case, the disturbance estimation signal $\mathbf{x}_{d1}$ allows to identify further disturbance effects, potentially affecting the controllable canonical plant.

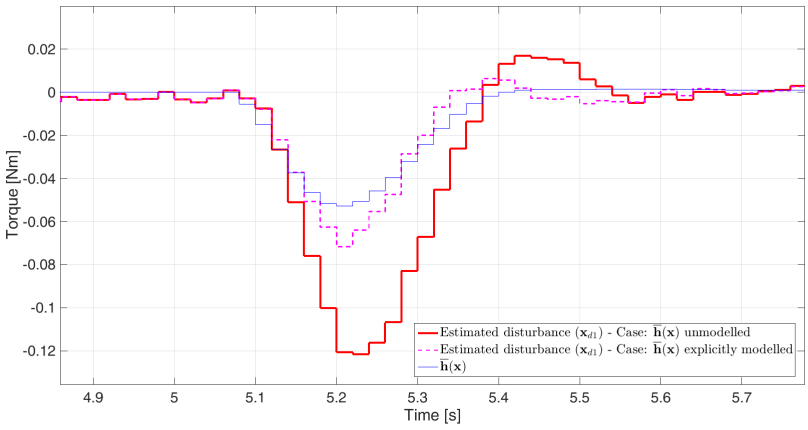

Figure 6: Disturbance estimation: simulation test.

Finally, we carried out a performance comparison between the controller developed in this study and a state-of-the-art high-performance UAV attitude controller [7], hereafter called the YU-SO(3) solution. The YU-SO(3) solution, based on an SO(3) formulation and three nested PID loops, was selected as a benchmark due to the very peculiar structure of its control law, and the capability to outperform most of the quadrotor attitude controllers known in literature [7].

In the simulated case here presented, an artificial torque disturbance was injected in the plant in order to unveil the discrepancies in the response of the two competing control laws, as well as their capability to properly and timely react in case of an unexpected disturbance input. Figure 7 depicts the two main results; concerning the ADRC-EMC disturbance estimation capability and the control laws performance comparison. Indeed, the disturbance signal (thin line) estimated by the rejector states (cf. x_{d1} in Fig. 1) is shown to suitably match, up to a certain bandwith, the true (simulated) disturbance (dashed-thin line) injected into the plant. Such a result helps to validate the disturbance estimation capabilities of the designed ADRC-EMC controller. In addition, Fig. 7 shows the control command, dispatched to the plant, both in the high-performance YU-SO(3) case (thick line), and in our ADRC-EMC design (thin line). It appears

that, our disturbance-based solution outperforms the YU-SO(3) control law. Indeed, in Fig. 7 we notice that the disturbance-based command departs from the saturation condition earlier than the YU-SO(3) one. In turn, this implies a faster response time, thus a lower tracking error in case of tricky manoeuvres (cf. also Fig. 8, along the manoeuvre time-interval). In addition, Fig. 8 compares the attitude tracking errors, for the two compared control laws, along the simulation trial depicted in Fig. 7. For the sake of clarity, only the roll angle is reported, being the one affected by the UAV simulated manoeuvre. We can notice how the ADRC-EMC control law behaves better in terms of tracking performance, during the action of the unexpected disturbance, as well as in the transient phase after the disturbance peak.

Most notably, the YU-SO(3) design required some non-trivial design capabilities and sharp design extensions. Indeed, the YU-SO(3) controller is augmented with a smith predictor, plus an adaptive gain adjuster, and a rotational trajectory planner, in order to enhance the performance [7]. What is more, the YU-SO(3) architecture uses a high-frequency measure of the quadrotor angular rate [7], hardly available in typical low-cost IMU sensors.

From these simulated results and considerations it can be thus inferred the compelling advantage of our disturbance-rejection-based approach: reducing the need for the designer to know the mathematical details of the plant to be controlled, while introducing several practical advantages and a more readily applicable solution.

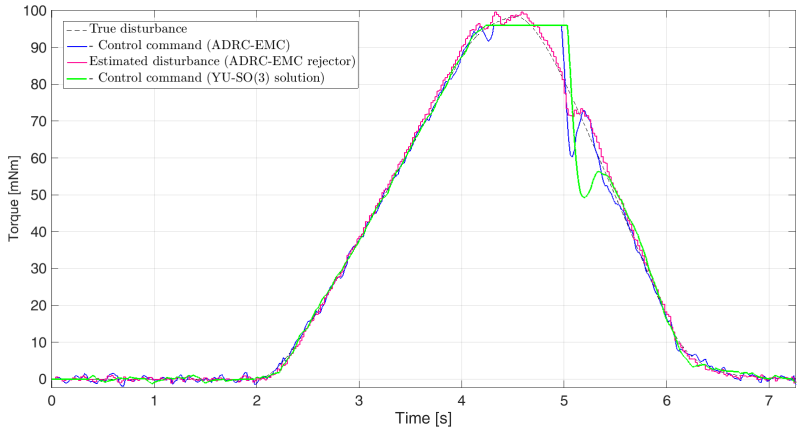

Figure 7: Command comparison, in the presence of saturation: simulation test.

4.3. Flight Tests

After the preliminary test-bench experiments, and a wide simulation campaign, the full three-axial attitude controller was tested in outdoor flight.

The outdoor attitude flight tests were organized in two sets of experiments, for analysis and safety purposes. In short, the first tests aimed at performing:

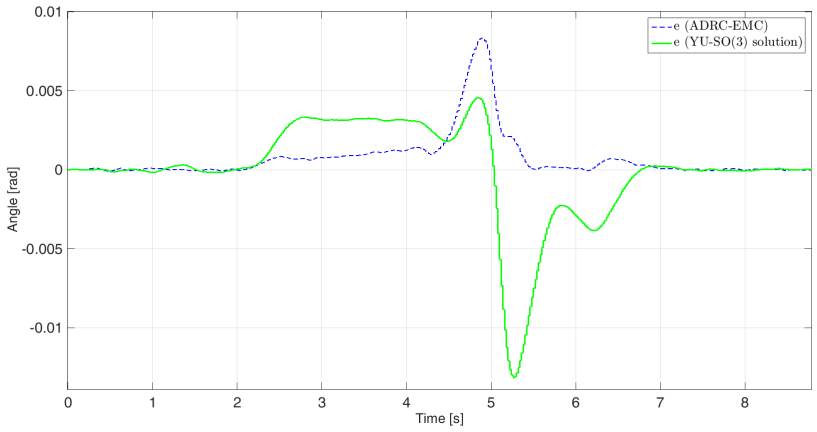

Figure 8: Attitude tracking errors comparison: simulation test.

take-off, attitude stabilization in hovering, and landing; and the UAV position was controlled by the operator, via a tilt reference.

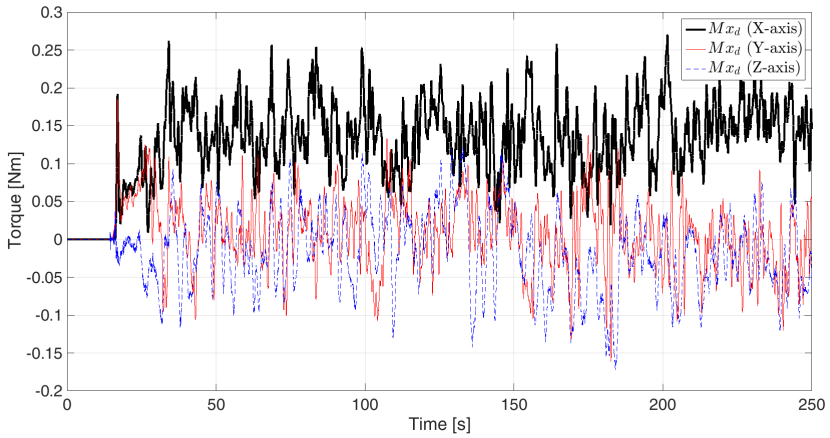

Figure 9: Attitude estimated disturbance: hovering flight test.

As an example, Fig. 9 and Fig. 10 depict the main outcomes of a 300 s hovering test. Specifically, Fig. 9 shows the real-time estimation of the rejector disturbance signals. As it can be noted, the X-axis disturbance (thick line) shows a mean value different from zero. Such a behaviour, implying a low-frequency torque disturbance, was supposed to be caused by an imbalance among the propellers' thrust. Further, in Fig. 10 the attitude roll and pitch angles trajectories are depicted, with an indication of both the reference (thick cross) and the average (thin cross) tilt. Since the tilt reference is set on-ground,

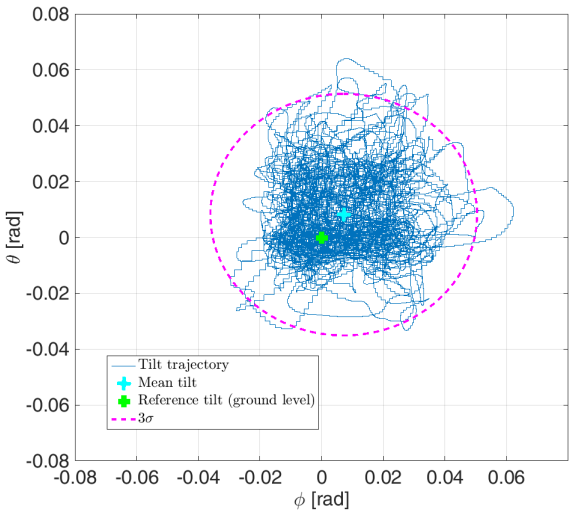

Figure 10: Attitude reference tracking: hovering flight test.

before the take-off, it is affected by the ground-level terrain inclination. Thus, a limited shift naturally occurs with respect to the average tilt; in hovering. Further, in Fig. 10 we notice how the tilt angles trajectories remain within the 3σ interval, with an average error smaller than 40 mrad. Such a result is coherent with the low-cost sensors and actuators leveraged in this study, as well as the quadrotor physical properties; as per Table 1. It can therefore be inferred that the attitude controller is able to enforce a quadrotor hovering flight. Most notably, the disturbance-based control unit is proven to be able to reject the disturbance effects showed in Fig. 9.

The second set of in-flight experiments aimed at testing the controller tracking performance, via horizontal flight manoeuvres; at moderate velocity. In this test configuration, the quadrotor tilt angles required by the displacement manoeuvre were limited to ± 0.25 rad, for safety reasons, yet coherently with the attitude mission scenario supposed and tested in Fig. 4. In addition, the quadrotor heading was controlled to zero.

In this scenario, Fig. 11 shows the attitude pitch angle trajectory (top) and the tilt angles tracking errors (bottom), for a UAV displacement along the X-body axis. During the flight, the horizontal peak acceleration reached $0.7\,\mathrm{m/s^2}$, whereas the maximum tilt angle was 0.211 rad. From the analysis of Fig. 11 there is evidence to indicate that the UAV attitude effectively tracks the guidance reference, according to the supposed quadrotor position displacement scenario.

In summary, the outcomes of the several experimental tests highlight a good attitude controller performance as well as validate to the greatest extent the proposed disturbance-rejection-based controller architecture. Interesingly, by

comparing Fig. 4 (bottom) and Fig. 11 (bottom), it can be also noticed that similar attitude manoeuvres, executed either on the test-bench or in-flight, lead appreciably to comparable attitude displacements and tracking errors.

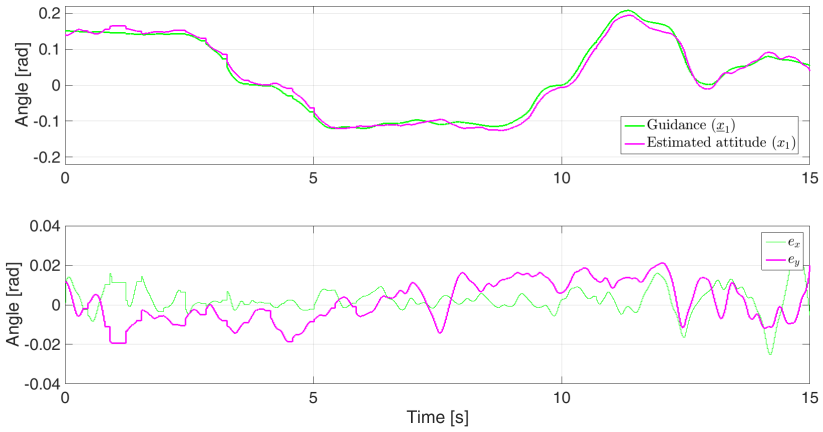

Figure 11: Flight test: pitch angle tracking (top), tilt tracking errors (bottom).

5. Conclusions

In summary, in this study the Active Disturbance Rejection Control (ADRC) design prescriptions were applied to the attitude control of a UAV quadrotor in combination with the Embedded Model Control (EMC) methodology, to extend the ADRC disturbance rejection capabilities and performance. Both ADRC and EMC are model-based control techniques leveraging an internal model of the plant, namely a simplified controllable model plus a disturbance rejector. However, the EMC peculiar disturbance design structure and tools, properly re-framed in the ADRC scenario, allow the proposed combined ADRC-EMC control unit to extend the typical ADRC structure along three lines.

We found that the model errors, introduced by neglecting the non-linear contributions of the model, may be either accurately estimated, via a tailored disturbance estimation dynamics, or dismissed, with a proper predictor tuning. Thus, our innovative ADRC-EMC rejector allowed to extend the validity of the simplified controllable model, in case of discrepancies between the model and the plant reality. As a result, a straightforward model-based control law was pursued, also capable of handling input disturbances entering the plant at multiple points.

Further, a multi-stage test procedure was implemented. Indeed, the combined ADRC-EMC attitude control unit was tested with a high-fidelity simulator, while a wide range of experimental tests were carried out via a single-axis test-bench, at first, and then in-flight. The findings indicate that the designed

ADRC-EMC control unit properly tracks the desired attitude trajectory, with the demanded performance level; even in presence of disturbances and kinematics couplings.

Finally, a simulated comparison, with respect to a state-of-the-art high-performance UAV attitude controller, brought further evidences about the design performance. What is more, the benchmark results strongly highlight the practical advantages of the proposed combined ADRC-EMC architecture in reducing, to a great extent, the complexity of the control problem, thus enhancing the applicability of the design solution and the potential impacts on engineering practice.

Acknowledgements

The authors would like to thank the anonymous reviewers for their helpful suggestions and remarks that contributed to improving the quality of the paper. They would also like to thank the Editors for their comments and support during the review process.

References

[1] M. A. Lotufo, L. Colangelo, C. Perez-Montenegro, E. Canuto, The feedback linearisation method for Embedded Model Control: The Borea project case-study, in: 2015 23rd Mediterranean Conference on Control and Automation (MED), IEEE, 2015, pp. 501–507. doi:10.1109/MED.2015.7158797.
URL http://ieeexplore.ieee.org/lpdocs/epic03/wrapper.htm?arnumber=7158797

[2] R. Mahony, V. Kumar, P. Corke, Multirotor aerial vehicles: Modeling, estimation, and control of quadrotor, IEEE Robotics and Automation Magazine 19 (3) (2012) 20–32. doi:10.1109/MRA.2012.2206474.

[3] A. Tayebi, S. McGilvray, Attitude stabilization of a VTOL quadrotor aircraft, IEEE Transactions on Control Systems Technology 14 (3) (2006) 562–571. doi:10.1109/TCST.2006.872519.

[4] N. Cao, A. F. Lynch, Inner–outer loop control for quadrotor uavs with input and state constraints, IEEE Transactions on Control Systems Technology 24 (5) (2016) 1797–1804.

[5] R. Naldi, M. Furci, R. G. Sanfelice, L. Marconi, Global trajectory tracking for underactuated vtol aerial vehicles using a cascade control paradigm, in: Decision and Control (CDC), 2013 IEEE 52nd Annual Conference on, IEEE, 2013, pp. 4212–4217.

[6] H. Bolandi, M. Rezaei, R. Mohsenipour, H. Nemati, S. M. Smailzadeh, Attitude control of a quadrotor with optimized pid controller.

[7] Y. Yu, S. Yang, M. Wang, C. Li, Z. Li, High performance full attitude control of a quadrotor on so(3), in: 2015 IEEE International Conference on Robotics and Automation (ICRA), 2015, pp. 1698–1703. doi:10.1109/ICRA.2015.7139416.

[8] J. Han, From pid to active disturbance rejection control, IEEE Transactions on Industrial Electronics 56 (3) (2009) 900–906. doi:10.1109/TIE.2008.2011621.

[9] M. Nakao, K. Ohnishi, K. Miyachi, A robust decentralized joint control based on interference estimation, in: Proceedings. 1987 IEEE International Conference on Robotics and Automation, Vol. 4, 1987, pp. 326–331. doi:10.1109/ROBOT.1987.1087996.

[10] W.-H. Chen, D. J. Ballance, P. J. Gawthrop, J. O'Reilly, A nonlinear disturbance observer for robotic manipulators, IEEE Transactions on Industrial Electronics 47 (4) (2000) 932–938. doi:10.1109/41.857974.

[11] M. Iwasaki, T. Shibata, N. Matsui, Disturbance-observer-based nonlinear friction compensation in table drive system, IEEE/ASME Transactions on Mechatronics 4 (1) (1999) 3–8. doi:10.1109/3516.752078.

[12] L. B. Freidovich, H. K. Khalil, Performance recovery of feedback-linearization-based designs, IEEE Transactions on Automatic Control 53 (10) (2008) 2324–2334. doi:10.1109/TAC.2008.2006821.

[13] E. Canuto, C. P. Montenegro, L. Colangelo, M. Lotufo, Active disturbance rejection control and embedded model control: a case study comparison, in: Control Conference (CCC), 2014 33rd Chinese, IEEE, 2014, pp. 3697–3702.

[14] Z. Gao, Active disturbance rejection control: a paradigm shift in feedback control system design, in: 2006 American Control Conference, 2006, pp. 7 pp.–. doi:10.1109/ACC.2006.1656579.

[15] Z. Gao, On the centrality of disturbance rejection in automatic control, ISA Transactions 53 (4) (2014) 850 – 857, disturbance Estimation and Mitigation. doi:https://doi.org/10.1016/j.isatra.2013.09.012.
URL http://www.sciencedirect.com/science/article/pii/S0019057813001559

[16] M. A. Lotufo, L. Colangelo, C. Perez-Montenegro, C. Novara, E. Canuto, Embedded model control for uav quadrotor via feedback linearization, IFAC-PapersOnLine 49 (17) (2016) 266–271.

[17] S. Zhao, Z. Gao, An active disturbance rejection based approach to vibration suppression in two-inertia systems, in: Proceedings of the 2010 American Control Conference, 2010, pp. 1520–1525. doi:10.1109/ACC.2010.5531284.

[18] E. Canuto, Embedded Model Control: outline of the theory., ISA transactions 46 (3) (2007) 363–77. doi:10.1016/j.isatra.2007.01.006.

[19] F. L. Markley, J. L. Crassidis, Fundamentals of spacecraft attitude determination and control, Vol. 33, Springer.

[20] M. A. Lotufo, C. Perez-Montegro, L. Colangelo, E. Canuto, C. Novara, Identification and control of a quadrotor from experimental data, in: Control and Automation (MED), 2016 24th Mediterranean Conference on, IEEE, 2016, pp. 895–900.

[21] R. C. Leishman, J. Macdonald, R. W. Beard, T. W. McLain, Quadrotors and accelerometers: State estimation with an improved dynamic model.